

Cluster Compounds

Pyrene-Terminated Tin Sulfide Clusters: Optical Properties and Deposition on a Metal Surface

Eugenie Geringer,^[a] Marina Gerhard,^[b] M. Koch,^[b] Claudio K. Krug,^[a] J. Michael Gottfried,^[a] and Stefanie Dehnen^{*[a]}

Abstract: Herein, we present the synthesis of two pyrene-functionalized clusters, $[(R^{pyr}Sn)_4S_6] \cdot 2CH_2Cl_2$ (**4**) and $[(R^{pyr}Sn)_4Sn_2S_{10}] \cdot nCH_2Cl_2$ ($n=4$, **5a**; $n=2$, **5b**; $R^{pyr} = CMe_2CH_2C(Me)N-NC(H)C_{16}H_9$), both of which form in reactions of the organotin sulfide cluster $[(R^N)Sn_4S_6]$ (**C**; $R^N = CMe_2CH_2C(Me)N-NH_2$) with the well-known fluorescent dye 1-pyrenecarboxaldehyde (**B**). In contrast, reactions using an organotin sulfide cluster with another core structure, $[(R^N)Sn_3S_4Cl]$ (**A**), leads to formation of small molecular frag-

ments, $[(R^{pyr}Cl_2Sn)_2S]$ (**1**), (pyren-1-ylmethylene)hydrazine (**2**), and 1,2-bis(pyren-1-ylmethylene)hydrazine (**3**). Besides synthesis and structures of the new compounds, we report the influence of the inorganic core on the optical properties of the dye, which was analyzed exemplarily for compound **5a** via absorption and fluorescence spectroscopy. This cluster was also used for exploring the potential of such non-volatile clusters for deposition on a metal surface under vacuum conditions.

Introduction

Pyrene-functionalized compounds are currently attracting much attention in materials research, as they combine many desirable properties for optoelectronic applications with a comparably easily achievable wide range of chemical modifications.

A large variety of organic pyrene-functionalized molecules have been presented in the literature,^[1] which show an overall high photoluminescence efficiency^[2] with a long singlet lifetime^[3] and a large Stokes shift. Furthermore, small changes in the environment can be monitored through shifts in position and intensity of the absorption and emission spectra of the molecules.^[4] These properties have led to the application of pyrene-functionalized compounds in organic dyads,^[5] in smart polymers,^[6] as chemical sensors,^[7] and labels for biomole-

cules.^[8] The high charge carrier mobility and excellent hole injection ability of the molecules have additionally led to applications in optoelectronic devices,^[9] like light-emitting diodes, organic field-effect transistors,^[10] or molecular switches and logic gates.^[11] Some organic–inorganic hybrid compounds have also been synthesized,^[12] with Sn-based molecules for possible application as catalysts^[13] or Fe-based molecules for electrochemical applications,^[14] and the attachment of pyrene ligands to surfaces has recently emerged as a means of tailoring optical properties of nanosized particles^[15] or for the functionalization of planar surfaces.^[16]

Still only a few examples of organic–inorganic hybrid compounds based on pyrene-functionalized inorganic cores have been known to date, although the combination with inorganic moieties allows for even more possibilities in tuning of the overall optoelectronic properties due to an enhanced structure-property relationship. Hence, fine-tuning of the bandgap energy, the electron affinity, emission pathways, or the strength of interactions with surfaces are achievable by adopting the chemical composition of the inorganic part of the compound.

In our work, we focus on the combination of semi-conductor-derived inorganic cluster structures with functional organic substituents. During the past decade, we have developed a family of C=O or C=NNH₂ functionalized organotin sulfide clusters, which serve as a versatile platform for the targeted extension of the organic ligands. The functionalities that are accessible this way vary from the provision of sufficient electron density for generating extreme non-linear optical properties,^[17] through the exposure of bio-organic groups,^[18] to chelate ligands that allow for the targeted trapping of metal ions.^[19] This approach also served to synthesize a variety of organotin sulfide compounds with aromatic ligands,^[20] which so far com-

[a] E. Geringer, Dr. C. K. Krug, Prof. Dr. J. M. Gottfried, Prof. Dr. S. Dehnen
 Fachbereich Chemie und Wissenschaftliches Zentrum für
 Materialwissenschaften (WZMW)
 Philipps-Universität Marburg
 Hans-Meerwein-Str. 4, 35043 Marburg (Germany)
 E-mail: dehnen@chemie.uni-marburg.de

[b] Dr. M. Gerhard, Prof. Dr. M. Koch
 Fachbereich Physik und Wissenschaftliches Zentrum für
 Materialwissenschaften (WZMW)
 Philipps-Universität Marburg
 Renthof 5, 35032 Marburg (Germany)

 Supporting information and the ORCID identification number(s) for the author(s) of this article can be found under:
<https://doi.org/10.1002/chem.202003889>.

 © 2020 The Authors. Published by Wiley-VCH GmbH. This is an open access article under the terms of Creative Commons Attribution NonCommercial License, which permits use, distribution and reproduction in any medium, provided the original work is properly cited and is not used for commercial purposes.

prised relatively small aromatic groups like phenyl, benzyl or naphthyl moieties,^[21] some heteroaromatic molecules like benzothiazole, furan, or quinolone^[21,22] or chelate ligands like bipyridyl or bispyridyl.^[23] According to our general approach, the attachment of these molecules succeeded through condensation reaction of the functionalized precursor clusters under mild conditions.

In order to introduce new overall optical properties into this family of compounds and at the same time facilitate an interaction with metal or semiconductor surfaces, we have expanded this idea towards an extended π -aromatic system under otherwise unchanged mild reaction conditions. For this purpose, we have chosen an organic residue that already possesses intriguing optical properties, while exhibiting a polycyclic aromatic structure. First studies into this direction were undertaken by reactions of the defect-heterocubane-based precursor cluster $[(R^N\text{Sn})_3\text{S}_4\text{Cl}]$ (**A**; $R^N = \text{CMe}_2\text{CH}_2\text{C}(\text{Me})\text{N-NH}_2$) with the well-known fluorescent dye 1-pyrenecarboxaldehyde (**B**). This procedure yielded small molecular compounds that allow for insight into the fragmentation processes during such reactions, $[(R^{Pyr}\text{Cl}_2\text{Sn})_2\text{S}]$ (**1**; $R^{Pyr} = \text{CMe}_2\text{CH}_2\text{C}(\text{Me})\text{N-NC}(\text{H})\text{C}_{16}\text{H}_9$), (pyren-1-ylmethylene)hydrazine (**2**), and 1,2-bis(pyren-1-ylmethylene)hydrazine (**3**). By using the „double-decker“-based precursor cluster $[(R^N\text{Sn})_4\text{S}_6]$ (**C**) instead, the reaction proceeded as planned, leading to the formation of two pyrene-functionalized clusters, $[(R^{Pyr}\text{Sn})_4\text{S}_6] \cdot 2\text{CH}_2\text{Cl}_2$ (**4**) and finally $[(R^{Pyr}\text{Sn})_4\text{Sn}_2\text{S}_{10}] \cdot n\text{CH}_2\text{Cl}_2$ ($n = 4$, **5a**; $n = 2$, **5b**), upon two or six days reaction time, respectively. All compounds were characterized by standard analytical methods (NMR spectroscopy, mass spectrometry) and were structurally determined by means of single-crystal X-ray diffraction. To probe the effect of the combination of these inorganic cluster moieties with the fluorescent dye, we studied the optical properties of compound **5** via UV-visible and photoluminescence spectroscopy, and we explored the compounds' ability to interact with solid surfaces.

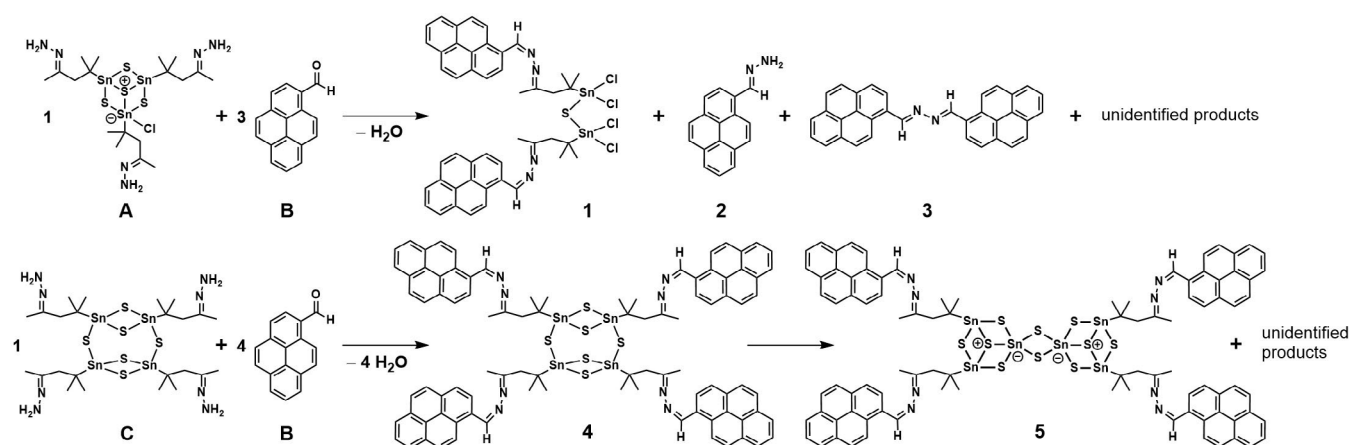
Results and Discussion

The reactions of the two precursor clusters $[(R^N\text{Sn})_3\text{S}_4\text{Cl}]$ (**A**) and $[(R^N\text{Sn})_4\text{S}_6]$ (**C**; $R^N = \text{CMe}_2\text{CH}_2\text{C}(\text{Me})\text{N-NH}_2$) with 1-pyrenecarboxaldehyde (**B**) under mild conditions, which led to the formation of compounds **1–5** under release of water are summarized in Scheme 1.

First, we tested the behavior of the known organotin sulfide cluster $[(R^N\text{Sn})_3\text{S}_4\text{Cl}]$ (**A**) in reactions with 1-pyrenecarboxaldehyde (**B**). Solutions of both starting materials were combined and stirred for three days. After layering with *n*-hexane, two different crystal types were obtained, comprising the compound $[(R^{Pyr}\text{Cl}_2\text{Sn})_2\text{S}]$ (**1**) ($R^{Pyr} = \text{CMe}_2\text{CH}_2\text{C}(\text{Me})\text{N-NC}(\text{H})\text{C}_{16}\text{H}_9$) and (pyren-1-ylmethylene)hydrazine (**2**). Compound **1** crystallizes in the monoclinic space group $P2_1/n$ with four formula units per unit cell. Compound **2** crystallizes in the triclinic space group $P\bar{1}$ with one molecule per unit cell.

The molecular structure of **1** (Figure 1, top) consists of two pyrene-terminated organotin groups that are connected by a sulfur atom and additionally bind two chloride ligands each for compensation of the charge. The Sn–S bonds lengths in **1** with 2.380(4) Å and 2.405(6) Å are in the range of Sn–S bond lengths of the starting material **A** (2.376(4)–2.645(7) Å),^[24] and the Sn–N distances with 2.380(6) Å and 2.407(8) Å are slightly elongated but similar to the Sn–N distances reported for a related ferrocene-functionalized molecule (2.336(1)–2.425(1) Å).^[25] The elongation of the Sn–N distance may be due to the size of the organic ligand. Although this structural motif is known for organotin sulfide clusters, it is not always isolable, but appears as intermediate during cluster formation according to NMR studies.^[24] Hence, its observation sheds light on the first steps in cluster rearrangement processes, which we anticipate to take place here, and which may help to understand the formation of compound **5** below.

Compound **2** (Figure 1, bottom left) most probably represents a follow-up product, which formed after the condensation reaction between the hydrazone-functionalized organotin sulfide cluster **A** and the 1-pyrenecarboxaldehyde (**B**) had al-



Scheme 1. Reaction of $[(R^N\text{Sn})_3\text{S}_4\text{Cl}]$ (**A**) and $[(R^N\text{Sn})_4\text{S}_6]$ (**C**) with 1-pyrenecarboxaldehyde (**B**), yielding compounds **1–5** discussed in this work. For clarity, the intramolecular Sn–N interactions in compounds **A**, **C**, **1**, **4** and **5** are not shown explicitly. Note that the scheme is not balanced in terms of the reaction stoichiometries.

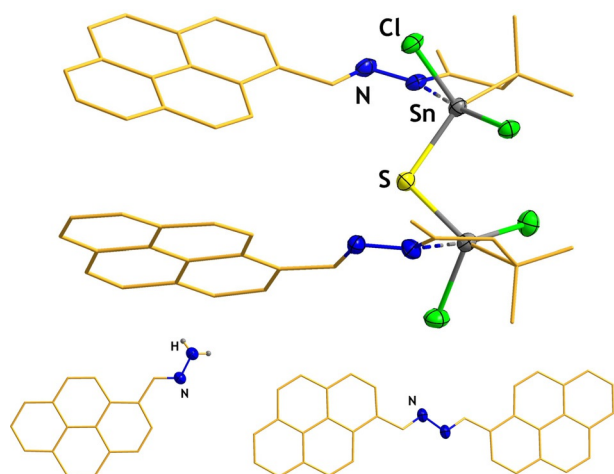


Figure 1. Molecular structure of compounds **1** (top), **2** (bottom, left), and **3** (bottom, right). Anisotropic displacement ellipsoids are drawn at 50% probability. Carbon atoms are drawn as wires, hydrogen atoms and solvent molecules are omitted for clarity.

readily taken place. This is indicated by the fact that **2** comprises a hydrazone group that stemmed from **A**. Hence, the release of the organic ligand included a C–N bond cleavage on the other side of the N=N unit. We extended the reaction time in order to potentially skip this intermediate state of the reaction. However, this led to the formation of yet another additional crystalline compound. Obviously, compound **2** is systematically released in this reaction mixture, and over time reacts with spare 1-pyrenecarboxaldehyde (**B**) to form the yet unprecedented dimer 1,2-bis(pyren-1-ylmethylene)hydrazine (**3**; Figure 1, bottom right).

These results indicate (a) a high tendency of the organotin sulfide precursor **A** toward fragmentation in this reaction system, and (b) a relatively low reactivity of the intermediates. We ascribe the latter to the presence of chloride ligands that serve to coordinatively saturate the tin atoms under formation of a neutral compound (an analogous compound with terminal sulfide ligands instead would be anionic). While the high fragmentation tendency would generally enable the formation of (larger) organotin sulfide clusters, the formation and crystallization of a relatively stable intermediate definitely serves to inhibit further cluster growth.

To overcome the early termination of the reaction, we thus chose to use another organotin sulfide precursor cluster without chloride ligands. Hence, a solution of **B** was added to a solution of another known compound, $[(R^N\text{Sn})_4\text{S}_6]$ (**C**; $R^N = \text{CMe}_2\text{CH}_2\text{C}(\text{Me})\text{N-NH}_2$). Upon stirring for two days, we observed the formation of the desired pyrene-functionalized derivative $[(R^{Py}\text{Sn})_4\text{S}_6] \cdot 2\text{CH}_2\text{Cl}_2$ (**4**) upon condensation reaction between the precursor compounds. Compound **4** crystallizes in the triclinic space group $P\bar{1}$ with one formula unit per unit cell.

The molecular structure of **4** (Figure 2, top) exhibits a virtually unchanged “double-decker”-like cluster topology with crystallographic inversion symmetry. The Sn–S bond lengths, ranging from 2.404(3) Å to 2.440(4) Å, are almost identical with those found in **C** (2.390(9)–2.514(2) Å),^[26] but the Sn...N distances

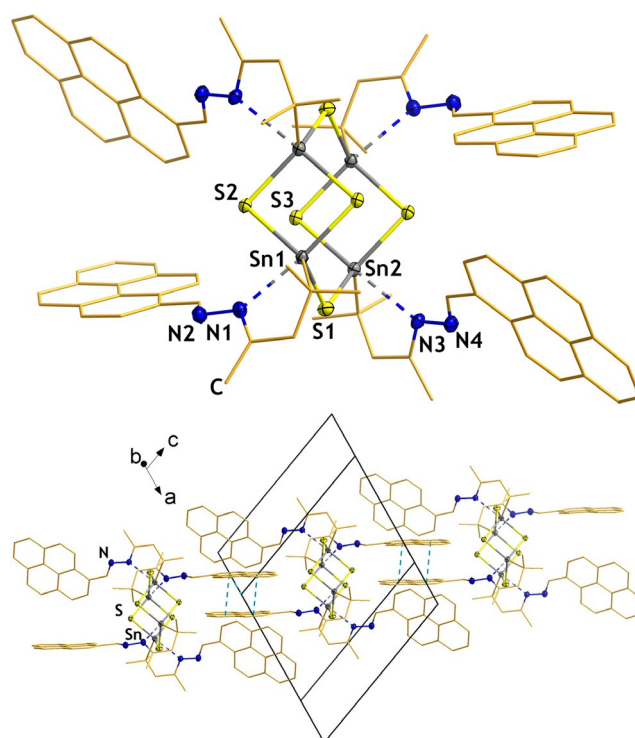


Figure 2. Molecular structure of compound **4** (top) and view of the packing of the molecules in the crystal (bottom). Anisotropic displacement ellipsoids are drawn at 50% probability. Carbon atoms drawn as wires, hydrogen atoms and solvent molecules are omitted for clarity. Contacts between ligand ring centroids are drawn as light blue dashed lines.

increased from 2.341(3)–2.391(02) Å in **C** to 2.530(9) Å and 2.571(0) Å in **4**. These values correspond to Sn...N distances observed in an organo-functionalized $\{\text{Sn}_2\text{S}_2\}$ four-membered ring exhibiting the same trigonal-bipyramidal coordination environment of the tin atoms (2.548(4) and 2.560(5) Å).^[27] The pyrene ligands are arranged in pairs at opposite sides of the inorganic cluster core. They are tilted towards each other by $64.3(5)^\circ$, indicative for the absence of notable intramolecular π -stacking interactions.

The crystal structure also indicates only weak intermolecular π -stacking, given that just a small part of one of the organic ligands of the asymmetric unit is able to overlap with its symmetry generated counterpart having centroid...centroid distances of 3.81(1) to 3.82(6) Å. The closest centroid...centroid distances between the other planarly oriented pyrene groups of adjacent clusters amount to 6.35(0) Å, clearly above the critical threshold of corresponding interactions.

After stirring for six days and subsequent layering with *n*-hexane, bright yellow crystals of $[(R^{Py}\text{Sn})_4\text{Sn}_2\text{S}_{10}] \cdot n\text{CH}_2\text{Cl}_2$ were obtained from the same solution with varying amount of co-crystallized solvent molecules ($n=4$, **5a**; $n=2$, **5b**) and different packing of the molecules within the crystal structure. **5a** crystallizes in the triclinic space group $P\bar{1}$ with one molecule per unit cell, **5b** crystallizes in the monoclinic space group $P2_1/c$ with two molecules per unit cell.

During the reaction, the inorganic cluster core undergoes a rearrangement from the initial “double-decker”-like topology

of **A** to form a μ -S-bridged dimer of defect-heterocubane-type cages (Figure 3 for **5a**, Figure S30 for **5b**). This kind of rearrangement is known to occur in functionalization reactions of **A** with expanded organic molecules.^[25,28] Along with this rearrangement, the Sn–S bond lengths partially increase from 2.390(9)–2.514(2) Å in **C** to 2.392(01)–2.731(9) Å in **5a** and 2.391(1)–2.879(03) Å in **5b**, which corresponds to the Sn–S bond lengths observed in molecules exhibiting a similar core structure (2.387(1)–2.755(3) Å).^[24] Whereas the Sn...N distances in **5a** (2.377(7)–2.392(05) Å) remain in the range of those found in the starting material (2.341(3)–2.391(2) Å), they partially increase in **5b** to be 2.374(7) Å and 2.621(2) Å. This is still in the expected range for Sn...N distances, and smaller than Sn...N distances in compounds with octahedrally coordinated tin atoms.^[29] The reason for the (partial) elongation of the

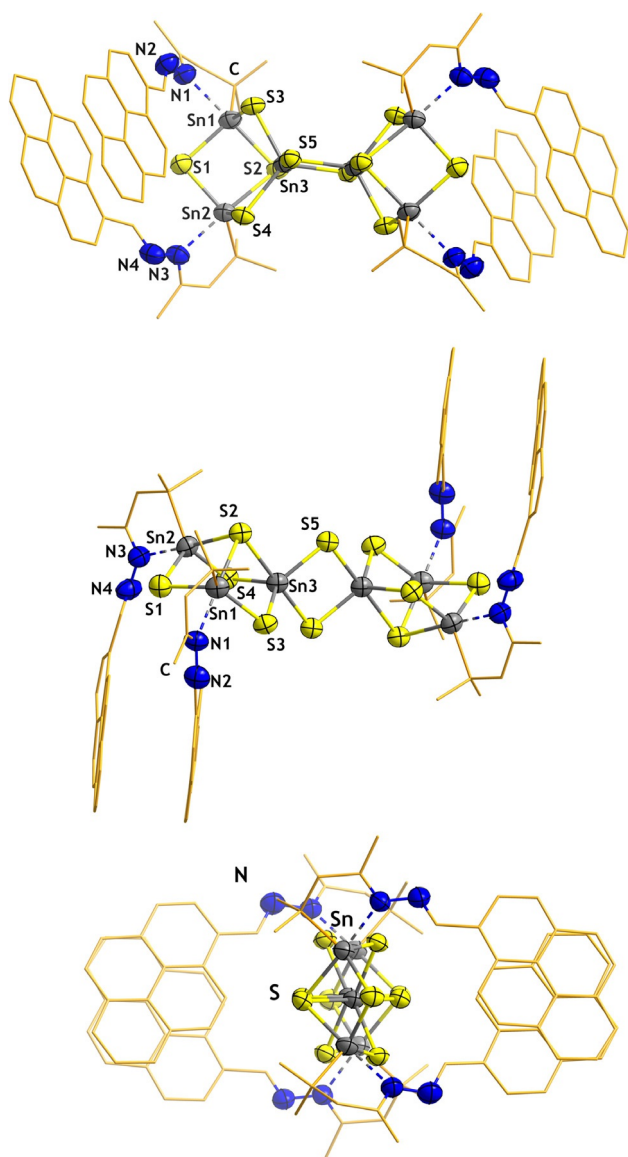


Figure 3. Molecular structure of compound **5** in three perpendicular views, shown for **5a** as an example. Anisotropic displacement ellipsoids are drawn at 50% probability. Carbon atoms are drawn as wires, hydrogen atoms and solvent molecules are omitted for clarity.

Sn...N distance may be the presence of a dichloromethane molecule relatively close to the organic group, even though the distance of 3.020(7) Å is too long as to be estimated as a significant hydrogen bond.

Since the inorganic core exhibits an elongated form, the four attached residues are divided into two groups of two substituents. The ligands of these two groups orient themselves away from each other but within the group, the ligands are aligned in an almost parallel fashion (deviation from co-planarity 4.05(1)°) with partial π -stacking. The intramolecular distances between the centroids of the aromatic rings range from 3.338(5) to 3.537(1) Å. In addition, the ligands are also aligned parallel to a ligand group of the neighboring molecule, at an intermolecular distance of 3.398(4)–3.881(6) Å between the organic molecules. This way, a chain of molecules is created, consisting of alternating organic and inorganic units (Figure 4).

The structure of the molecule in **5b** (see Figure S30) is almost identical with that observed in compound **5a**. Again, the pairs of organic ligands are *trans*-disposed with respect to the cluster core in opposite directions, and the ligands are aligned almost parallel to each other and also to a neighboring ligand group. The intramolecular distances between the aromatic ligands range from 3.327(8) to 3.920(6) Å and the intermolecular ones from 3.344(8) to 3.912(5) Å. The comparably broader ranges of both types of distances result from the slightly larger deviation of the ligand orientation from co-planarity (5.07(7)°). Yet, the stacking of the organic ligands again leads to the formation of a chain-like arrangement with alternating organic and inorganic units. The difference between the crystal structures of **5a** and **5b** is found in the packing of

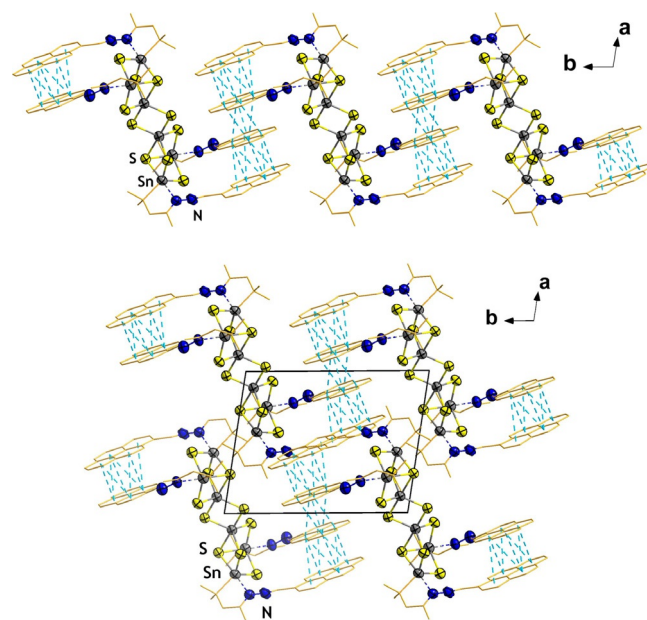


Figure 4. Top: Chain of molecules upon intense π -stacking between the pyrene groups in the crystal structure of compound **1a**. Bottom: packing of molecules in the crystal structure of **1a**. Anisotropic displacement ellipsoids are drawn at 50% probability. Carbon atoms are drawn as wires, hydrogen atoms and solvent molecules are omitted for clarity. Contacts between ligand ring centroids are drawn as light blue dashed lines.

these chains within the crystal structure. While all chains are oriented the same way in **5a**, they are arranged in two layers with a tilt of $22.346(8)^\circ$ between the layers in **5b** (see Figure S32).

We like to note that, while the rearrangement of the smaller $\{\text{Sn}_4\text{S}_6\}$ core to form the larger $\{\text{Sn}_6\text{S}_{10}\}$ is very typical for functionalization reactions of organotin sulfide compounds with large organic substituents, the observation of both, the unchanged and the rearranged version is rare. The rearrangement of the cluster core enlarges the space between the substituents, which explains the preference of this process. Hence, the appearance of both topologies in this case shows that both can indeed coexist within one reaction solution, but the larger clusters seem to be more stable over time.

We chose compound **5** for investigating further properties of the novel pyrene-functionalized organotin clusters, as the intense π -stacking seemed to allow for excimer formation (see below) and also for a relatively large degree of order of the organic substituents as a helpful precondition for deposition on substrates.

To investigate the optical properties of compound **5**, UV-visible and photoluminescence (PL) measurements were performed. For this purpose, crystalline samples of **5** and the starting material 1-pyrenecarboxaldehyde (**B**) were analyzed under inert gas conditions (argon). The resulting UV-visible spectra, displayed in Figure 5, show that 1-pyrenecarboxaldehyde (**B**) absorbs light with wavelengths below 500 nm (from an energy of about 2.48 eV upwards), with characteristic features in the region of 321 nm to 419 nm (2.96–3.86 eV)^[5b,30] and a steep increase of absorbance below these. The absorption of compound **1** has an onset around 527 nm (2.35 eV) and is thus shifted by 27 nm (0.13 eV) towards lower energies. In addition, the characteristic features of **B** are smoothed in the spectrum of compound **5**, and result in a weaker absorbance level in this region and a sharp increase in absorption at 329 nm (3.77 eV) corresponding to the steep increase observed for **B**. The

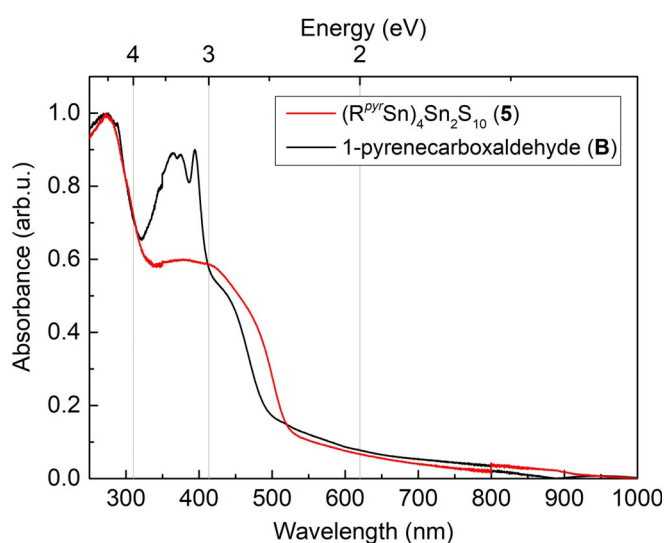


Figure 5. UV-visible spectra of **B** and **5**, measured in diffuse reflectance on pulverized single crystals under argon atmosphere.

change of the characteristic region shows the influence of the inorganic core and can be taken as an indicator for electronic communication between the ligands and the cluster core leading to a reduced probability of the optical transition of the organic Ligand.

The PL spectra of the same compounds are shown in Figure 6. **B** exhibits a broad emission of light between 470 nm and 750 nm, with a maximum around 570 nm upon excitation with 405 nm, which fits to literature.^[31] The spectrum of compound **5** is similar to the previous one, as the sample emits

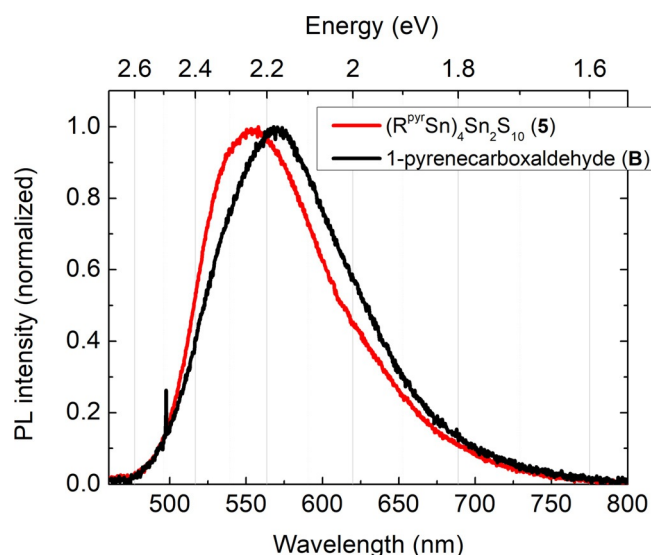


Figure 6. Photoluminescence spectra of **B** and **5**. For **B**, the excitation wavelength was 405 nm with an excitation power of 0.42 mW and for **5**, an excitation wavelength of 440 nm with an excitation power of 0.5 mW was applied.

light from 475 nm up to 750 nm, with its maximum at ca. 555 nm. The PL spectra measured on the organic molecule alone and upon attachment to the cluster have slightly shifted maxima in the intensity, but both cover almost the complete visible range and have similar curve shapes. This shows that the photoluminescence properties of the organic ligand are retained when attached to the tin sulfide core. According to the literature, the broad emission in this range can be assigned to an emission of an excited dimer of pyrene-groups (“excimers”).^[3a,4a] The presence of excimers is expected in this case, as the measurements were carried out on single-crystalline samples, in which intense π -stacking of pyrene-groups was observed.

In a first attempt to deposit (non-volatile) organotin sulfide clusters onto a surface under vacuum conditions, we prepared a solution of **5** in CH_2Cl_2 (0.5 mmol L^{-1}) and sprayed it onto a clean Au(111) surface in a vacuum system using a pulse valve (see the Experimental Section for details). X-ray photoelectron (XP) spectra taken after deposition of 20 pulses are displayed in Figure 7. The survey spectrum (Figure 7a) shows the signals of all constituting elements and of some minor contaminants. Detailed XP spectra of selected binding energy regions are presented in Figure 7b–e and in Figure S36. The signals of the

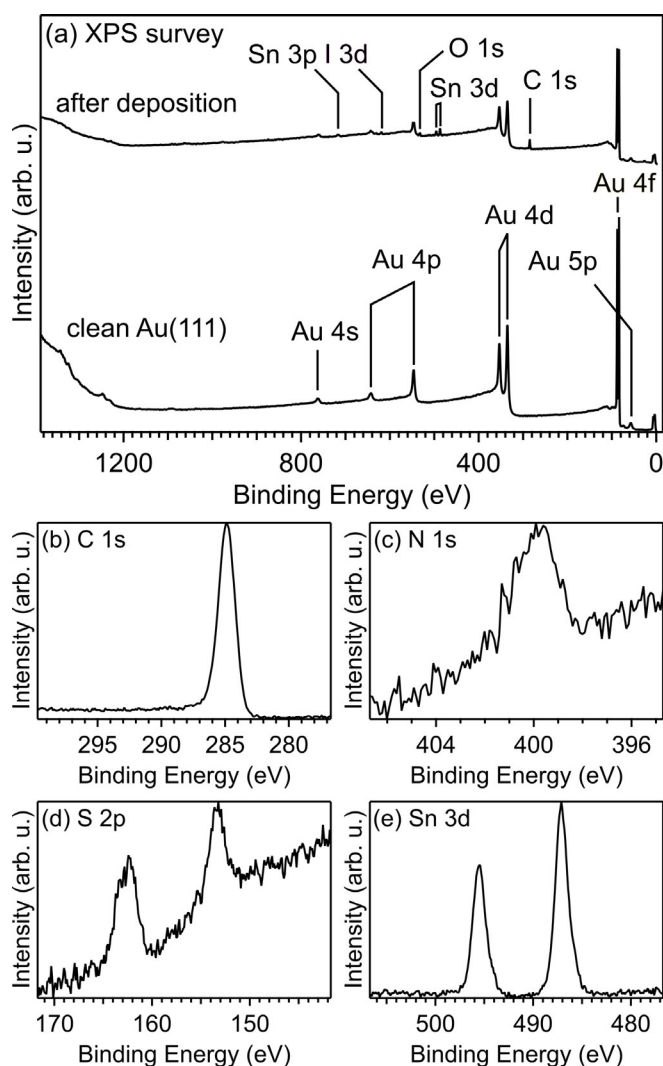


Figure 7. XP spectra taken after vacuum spray deposition of **5** onto a Au(111) surface from CH_2Cl_2 solution. (a) Survey spectra of the clean Au(111) surface (bottom) and after deposition of **5** (top), showing additional signals corresponding to the elements present in **5** (C, N, S, and Sn) as well as some contaminations (O, I). High-resolution spectra of selected binding energy regions: (b) C 1s, (c) N 1s, (d) S 2p, (e) Sn 3d.

constituting elements appear in the expected binding energy ranges characteristic for the bonding situation in the molecule, indicating that deposition of the intact compound on a metal surface is possible. While the asymmetry of the N 1s signal may indicate partial decomposition, it is more likely caused by interaction of the N atoms in the molecule with different adsorption sites and in different adsorption geometries. This is supported by corresponding scanning tunneling microscopy (STM) images (Figures S37 and S38), which reveal a largely disordered layer. Because of the conformational flexibility of the molecules, many different adsorption configurations are expected. Indeed, while the images exhibit features in the right order of magnitude of the pyrene units, the variability of appearance makes it impossible to identify individual molecules. We assume that the molecules cannot dock to the surface with all four pyrene groups at a time owing to geometrical restrictions by the cluster structure. As a consequence, there are

many possible variations of attachment modes for varying numbers of pyrene units in a cluster molecule.

Conclusions

In this contribution, we presented the synthesis and single crystal structure of a first series of organotin sulfide compounds that were functionalized with pyrene units to modify the optical absorption properties of the clusters, introduce fluorescence properties to them, and allow for interaction with solid surfaces. Compounds $[(\text{R}^{\text{pyr}}\text{Cl}_2\text{Sn})_2\text{S}]$ (**1**), (pyren-1-ylmethylene)hydrazine (**2**), 1,2-bis(pyren-1-ylmethylene)hydrazine (**3**), $[(\text{R}^{\text{pyr}}\text{Sn})_4\text{S}_6] \cdot 2\text{CH}_2\text{Cl}_2$ (**4**), and $[(\text{R}^{\text{pyr}}\text{Sn})_4\text{S}_2\text{S}_{10}]$ (**5**) were obtained in single-crystalline form from reactions of hydrazone-functionalized organotin sulfide clusters with the 1-pyrenecarboxaldehyde (**B**). We identified a general difference in the product spectrum when using $[(\text{R}^{\text{N}}\text{Sn})_3\text{S}_4\text{Cl}]$ (**A**; $\text{R}^{\text{N}} = \text{CMe}_2\text{CH}_2\text{C}(\text{Me})\text{N-NH}_2$) or $[(\text{R}^{\text{N}}\text{Sn})_4\text{S}_6]$ (**C**), respectively, as precursor clusters. We ascribe the observation of small molecular fragments **1**, **2**, and **3** upon reactions using **A** to the presence of chloride ligands in this starting compound. In contrast, reactions that start out from **C** lead to the desired products upon condensation reactions at the original substituents, which are extended by the pyrene units this way. We could show that the reactions proceed in a way that allows the isolation of a cluster with unchanged tin sulfide cluster core (**4**) upon two days, whereas a rearrangement of the core structure and crystallization of a larger cluster (**5**) occurred after prolonged reaction time. The latter is typical for the presence of bulky organic substituents at such clusters, hence the intermediate occurrence of the unchanged version is a rare observation.

Both cluster types show significant differences in the relative orientation of the pyrene groups, with significantly more pronounced π -stacking in the case of **5**. We therefore analyzed this compound's optical properties and could show that there seems to be a communication between the organic dye and the tin sulfide cluster core, which influences the absorption properties of the pyrene moiety, while the fluorescence properties inherited from the pyrene ligand are essentially unchanged relative to the parent compound **B**. In addition, XPS and STM measurements gave first evidence towards successful neutral-spray vacuum deposition of the cluster molecules on a gold surface, resulting in a disordered layer with large variability in conformational adaptation. Future investigations will include further polycyclic aromatic and related polycyclic compounds in order to further enhance optical properties and the quality of thin cluster layers on planar surfaces.

Experimental Section

General: All synthesis steps were carried out under dry argon atmosphere with exclusion of air and moisture. All solvents were purified and dried prior to use. $[(\text{R}^{\text{N}}\text{Sn})_3\text{S}_4\text{Cl}]$ (**A**) and $[(\text{R}^{\text{N}}\text{Sn})_4\text{S}_6]$ (**C**) ($\text{R}^{\text{N}} = \text{CMe}_2\text{CH}_2\text{C}(\text{Me})\text{N-NH}_2$) were synthesized according to procedures reported in the literature.^[26,32] Further chemicals were purchased from Sigma–Aldrich and used as received.

Synthesis of [(R^{pyr}Cl₂Sn)₂] (**1**; R^{pyr} = CMe₂CH₂C(Me)N-NC(H)C₁₆H₉), **(pyren-1-ylmethylene)hydrazine** (**2**), and **1,2-bis(pyren-1-ylmethylene)hydrazine** (**3**). [(R^NSn)₃S₄Cl] (**A**; R^N = CMe₂CH₂CMeN-NH₂; 105 mg, 0.128 mmol) was dissolved in 10 mL of CH₂Cl₂ (dichloromethane, DCM) and added to a solution of 1-pyrenecarboxaldehyde (123 mg, 0.538 mmol) in 10 mL of DCM. The bright yellow mixture was stirred for 3 d at room temperature. Layering of the solution with *n*-hexane (1:1.5) yielded pale yellow, block-shaped crystals of **1** and bright yellow plates of **2**. Stirring for any additional amount of time leads to additional crystallization of **3**. For **1** and **2**, no evidence of ions was found by mass spectrometry, attributed to either low concentration or low stability at ionization conditions. For **3**) HRMS (LIFDI): *m/z* calcd.: 456.16265 [M]⁺ found: 456.16512. NMR data of **1** could not be measured, as the (intermediate) compound was obviously not stable in solution. By-products **2** and **3** were not further investigated besides X-ray diffraction and LIFDI mass spectrometry.

Synthesis of [(R^{pyr}Sn)₄S₆]·2CH₂Cl₂ (**4**; R^{pyr} = CMe₂CH₂C(Me)N-NC(H)C₁₆H₉); [(R^NSn)₄S₆] (**C**; R^N = CMe₂CH₂CMeN-NH₂; 100 mg, 0.089 mmol) was dissolved in 15 mL of DCM and added to a solution of 1-pyrenecarboxaldehyde (93 mg, 0.405 mmol) in 10 mL of DCM. The bright yellow mixture was stirred for 48 h at room temperature. Layering of the solution with *n*-hexane (1:1.5) yielded bright yellow, block-shaped crystals of **4**. ¹H NMR (300 MHz, CDCl₃, 25 °C): δ = 10.72 (s, 1H, C(N)H), 9.32 (d, *J* = 9.3 Hz, 1H), 8.35 (d, *J* = 8.0 Hz, 1H), 8.27–8.19 (m, 3H), 8.15 (d, *J* = 9.0 Hz, 2H), 8.03 (dd, *J* = 15.1, 8.2 Hz, 2H), 2.52 (s, 1H), 1.90–1.71 (m, 2H), 1.43–1.20 (m, 4H). ¹³C NMR (75 MHz, CDCl₃) δ = 193.05, 152.51, 135.53, 131.34, 131.08, 131.00, 130.82, 130.72, 130.47, 129.03, 127.46, 127.24, 127.10, 126.88, 126.61, 124.66, 124.58, 124.08, 123.03, 53.54, 51.13, 26.70, 16.74; note that a ¹¹⁹Sn NMR spectrum of compound **4** could not be recorded owing to the extremely low solubility of the crystals and too low concentration of **4** in the reaction solution due to either immediate crystallization upon formation or further reaction to **5**. HRMS (ESI⁺): *m/z* calcd.: 1461.1077 [M]⁺ found: 1461.1031.

Synthesis of [(R^{pyr}Sn)₄Sn₂S₁₀]·*n*CH₂Cl₂ (*n* = 4, **5a**; *n* = 2, **5b**; R^{pyr} = CMe₂CH₂C(Me)N-NC(H)C₁₆H₉); [(R^NSn)₄S₆] (**C**; R^N = CMe₂CH₂CMeN-NH₂; 100 mg, 0.089 mmol) was dissolved in 15 mL of DCM and added to a solution of 1-pyrenecarboxaldehyde (93 mg, 0.405 mmol) in 10 mL of DCM. The bright yellow mixture was stirred for 6 d at room temperature. Layering of the solution with *n*-hexane (1:1.5) yielded bright yellow, block-shaped crystals of **5a** and **5b** in approx. 60% yield. Both solvates are indistinguishable with the naked eye by microscopy. ¹H NMR (300 MHz, CD₂Cl₂, 25 °C): δ = 10.77 (s, 1H, C(N)H), 9.41 (d, *J* = 9.4 Hz, 1H), 8.46 (d, *J* = 8.0 Hz, 1H), 8.31 (ddd, *J* = 19.6, 8.4, 5.7 Hz, 5H), 8.16–8.06 (m, 2H), 2.49 (s, 2H, CH₂), 1.78 (s, 3H, CH₃, CMe), 1.32 (s, 6H, CH₃, CMe₂) ppm. ¹³C NMR (75 MHz, CD₂Cl₂, 25 °C): δ = 193.04, 152.19, 135.64, 131.44, 131.16, 131.07, 130.86, 130.77, 130.60, 127.73, 127.36, 127.21, 126.93, 126.78, 124.77, 123.09, 50.88, 36.46, 26.34, 16.49, 0.90. ¹¹⁹Sn NMR (187 MHz, CD₂Cl₂, 25 °C): δ = -114 ppm; owing to the poor solubility of the compound the signal-to-noise ratio is very low, hence the signal is very weak; we take this as an explanation for the observation of the stronger signal only, instead of two signals with relative intensities of 2:1 that would be expected according to different chemical environments of Sn1 and Sn2 as compared to Sn3. HRMS (ESI⁺): *m/z* calcd.: 2333.8173 [M]⁺ found: 2333.8665.

Spectroscopy and spectrometry: ¹H NMR spectra were recorded on a Bruker AVII 300 spectrometer at 300 K. ¹H, ¹³C, and ¹¹⁹Sn NMR spectra were recorded with a Bruker AVIII 500 spectrometer. Electrospray-ionization (ESI) mass spectra were recorded with a Finnigan LTQ-FT Ultra mass spectrometer from Thermo Fischer Scientific.

The resolution was set to 100,000. All samples were handled under argon and dissolved in dry solvents. Hamilton syringes (250 μL) were used for sample injection via syringe pump infusion. Liquid injection field desorption/ionization (LIFDI) mass spectra were recorded with an AccuTOF GCv 4G from JOEL Time of flight (TOF) mass spectrometer. An internal or external standard was used for drift time correction. The LIFDI ion source was purchased from Linden ChromaSpec GmbH (Bremen, Germany).

X-ray diffraction and structure analysis: Single-crystal X-ray structure data of compounds **1**, **2**, **4** and **5a** was measured on a STOE IPDS 2T diffractometer applying a Mo-Kα X-ray source (λ = 0.71073 Å). Single-crystal X-ray structure data of compounds **3** and **5b** was measured using a STOE StadiVari diffractometer applying a Cu-Kα X-ray radiation source (λ = 1.54186). All measurements were carried out at 100 K. Reflection Data were processed with X-Area 1.^[33] The structures were solved by intrinsic Phase methods in SHELXT^[34] and refined by full-matrix-least-squares refinement against F² in SHELXL^[35] using the Olex2^[36] user interface.

Deposition Numbers 2022910, 2022911, 2022912, 2022913, 2022914, and 2022915 (**1**, **2**, **3**, **4**, **5a**, and **5b**) contain(s) the supplementary crystallographic data for this paper. These data are provided free of charge by the joint Cambridge Crystallographic Data Centre and Fachinformationszentrum Karlsruhe Access Structures service.

UV-visible spectroscopy: Measurements were carried out on a Agilent Cary 5000 with a Praying Mantis Diffuse Reflectance Accessory. Samples were prepared inside an argon glovebox and placed in a sealable sample holder for measurements.

Photoluminescence spectroscopy (PL): Photoluminescence spectroscopy was carried out in two different experimental setups: For compound **5**, the frequency doubled output of a titanium sapphire laser at 440 nm was used and compound **B** was excited with the 405 nm output of a diode laser. The different excitation conditions are not assumed to have any influence on the emission characteristics of the material. In both cases luminescence spectra were detected with a USB spectrometer (Ocean Optics). More PL spectra of different crystals are presented in the supplemental material (see Figure S35 for details).

X-ray photoelectron spectroscopy (XPS) and scanning tunneling microscopy (STM): The XPS and STM experiments were performed in a ultrahigh-vacuum apparatus (base pressure in the low 10⁻¹⁰ mbar range), equipped with a monochromated Al-Kα X-ray source (1486.7 eV), three-grid low-energy electron diffraction (LEED) optics (SPECS ErLEED 1000A), a SPECS Phoibos 150 electron energy analyzer, a SPECS STM 150 Aarhus, and a preparation chamber. The Au(111) single-crystal sample was prepared by repeated cycles of Ar⁺ ion bombardment (500 eV) and annealing (800 K). Surface cleanliness and long-range order were confirmed by X-ray photoelectron spectroscopy (XPS) and LEED, respectively. Deposition of the molecules was performed in UHV by spraying a solution (0.5 mmol L⁻¹ in CH₂Cl₂) into the vacuum using a pulse valve (Atomic Layer Deposition ALI-1000 by BihurCrystal).

Acknowledgements

This work was supported by the Deutsche Forschungsgemeinschaft (DFG) within the framework of SFB 1083. The authors thank Yasmeen Al Hamood Al Bisher for her assistance with the PL measurements. Open access funding enabled and organized by Projekt DEAL.

Conflict of interest

The authors declare no conflict of interest.

Keywords: fluorescence · optical absorption · hybrid compounds · organotin sulfide clusters · pyrene ligands

- [1] a) D. Zych, *Molecules* **2019**, *24*, 2551–2583; b) F. Dumur, *Eur. Polym. J.* **2020**, *126*, 109564; c) T. M. Figueira-Duarte, K. Müllen, *Chem. Rev.* **2011**, *111*, 7260–7314; d) Y. Ohishi, M. Inouye, *Tetrahedron Lett.* **2019**, *60*, 151232; e) Z. Jin, D. Wang, X. Wang, P. Liang, Y. Mi, H. Yang, *Tetrahedron Lett.* **2013**, *54*, 4859–4864.
- [2] a) U. Reeta Felscia, B. J. M. Rajkumar, M. B. Mary, *J. Mater. Sci.* **2018**, *53*, 15213–15225; b) H. Maeda, T. Maeda, K. Mizuno, K. Fujimoto, H. Shimizu, M. Inouye, *Chem. Eur. J.* **2006**, *12*, 824–831.
- [3] a) J. Illescas, C. Caicedo, G. Zaragoza-Galán, Y. S. Ramírez-Fuentes, A. Ge-lover-Santiago, E. Rivera, *Synth. Met.* **2011**, *161*, 775–782; b) R. Katoh, S. Sinha, S. Murata, M. Tachiya, *J. Photochem. Photobiol. A* **2001**, *145*, 23–34.
- [4] a) F. M. Winnik, *Chem. Rev.* **1993**, *93*, 587–614; b) S. Sarkar, S. Roy, A. Sikdar, R. N. Saha, S. S. Panja, *Analyst* **2013**, *138*, 7119–7126; c) J. Hoche, H.-C. Schmitt, A. Humeniuk, I. Fischer, R. Mitrić, M. I. S. Röhr, *Phys. Chem. Chem. Phys.* **2017**, *19*, 25002–25015.
- [5] a) A. Karuppusamy, P. Kannan, *J. Lumin.* **2018**, *194*, 718–728; b) P. K. Poddutoori, B. G. Maiya, *Indian J. Chem.* **2003**, *42A*, 2198–2204; c) J. Qiu, A. Hameau, X. Shi, S. Mignani, J.-P. Majoral, A.-M. Caminade, *ChemPlusChem* **2019**, *84*, 1070–1080.
- [6] a) A. Farcas, I. Ghosh, W. M. Nau, *Chem. Phys. Lett.* **2012**, *535*, 120–125; b) P. Somerharju, *Chem. Phys. Lipids* **2002**, *116*, 57–74; c) J. Duhamel, *Langmuir* **2012**, *28*, 6527–6538.
- [7] a) H. Kim, B. A. Rao, Y.-A. Son, *Fibers Polym.* **2013**, *14*, 2010–2014; b) Y. Yang, X. Gou, J. Blecha, H. Cao, *Tetrahedron Lett.* **2010**, *51*, 3422–3425; c) Y. Jeong, J. Yoon, *Inorg. Chim. Acta* **2012**, *381*, 2–14; d) S. Karuppannan, J.-C. Chambron, *Chem. Asian J.* **2011**, *6*, 964–984; e) S. Shanmugara-ju, P. S. Mukherjee, *Chem. Commun.* **2015**, *51*, 16014–16032.
- [8] a) M. Mariappan, B. G. Maiya, *Eur. J. Inorg. Chem.* **2005**, 2164–2173; b) M. E. Østergaard, P. J. Hrdlicka, *Chem. Soc. Rev.* **2011**, *40*, 5771–5788; c) G. Bains, A. B. Patel, V. Narayanaswami, *Molecules* **2011**, *16*, 7909–7935.
- [9] a) T. Zhang, J. Ye, A. Luo, D. Liu, *Opt. Mater.* **2020**, *100*, 109632; b) S. Diring, F. Camerel, B. Donnio, T. Dintzer, S. Toffanin, R. Capelli, M. Muccini, R. Ziessel, *J. Am. Chem. Soc.* **2009**, *131*, 18177–18185.
- [10] Y. Gong, X. Zhan, Q. Li, Z. Li, *Sci. China Chem.* **2016**, *59*, 1623–1631.
- [11] R. Canton-Vitoria, Y. Sayed-Ahmad-Baraza, M. Pelaez-Fernandez, R. Arenal, C. Bittencourt, C. P. Ewels, N. Tagmatarchis, *NPJ 2D Mater. Appl.* **2017**, *1*, 850.
- [12] a) A. Coleman, M. T. Pryce, *Inorg. Chem.* **2008**, *47*, 10980–10990; b) M. Braun, W. Tuffentsammer, H. Wachtel, H. C. Wolf, *Chem. Phys. Lett.* **1999**, *307*, 373–378.
- [13] D. Stien, S. Gastaldi, *J. Org. Chem.* **2004**, *69*, 4464–4470.
- [14] O. A. Varzatskii, D. A. Oranskiy, S. V. Vakarov, N. V. Chornenka, A. S. Belov, A. V. Vologzhanina, A. A. Pavlov, S. A. Grigoriev, A. S. Pushkarev, P. Millet, V. N. Kalinichenko, Y. Z. Voloshin, A. G. Dedov, *Int. J. Hydrogen Energy* **2017**, *42*, 27894–27909.
- [15] a) G. Battistini, P. G. Cozzi, J.-P. Jalkanen, M. Montalti, L. Prodi, N. Zacheroni, F. Zerbetto, *ACS Nano* **2008**, *2*, 77–84; b) A. Picard-Lafond, J.-F. Morin, *Langmuir* **2017**, *33*, 5385–5392; c) S. R. King, S. Shimmon, D. D. Totonjian, A. M. McDonagh, *J. Phys. Chem. C* **2017**, *121*, 13944–13951.
- [16] a) T. A. Pham, F. Song, M.-T. Nguyen, M. Stöhr, *Chem. Commun.* **2014**, *50*, 14089–14092; b) D. K. Perivoliotis, Y. Sato, K. Suenaga, N. Tagmatarchis, *Chem. Eur. J.* **2019**, *25*, 11105–11113; c) R. Canton-Vitoria, Y. Sayed-Ahmad-Baraza, B. Humbert, R. Arenal, C. P. Ewels, N. Tagmatarchis, *Nanomaterials* **2020**, *10*, 363–378.
- [17] a) K. Hanau, S. Schwan, M. R. Schäfer, M. J. Müller, C. Dues, N. Rinn, S. Sanna, S. Chatterjee, D. Mollenhauer, S. Dehnen, *Angew. Chem. Int. Ed.* **2020**, *59*, <https://doi.org/10.1002/anie.202011370>; *Angew. Chem.* **2020**, *132*, <https://doi.org/10.1002/ange.202011370>; b) E. Dornsiepen, F. Dobener, S. Chatterjee, S. Dehnen, *Angew. Chem. Int. Ed.* **2019**, *58*, 17041–17046; *Angew. Chem.* **2019**, *131*, 17197–17202; c) E. Dornsiepen, F. Dobener, N. Mengel, O. Lenchuk, C. Dues, S. Sanna, D. Mollenhauer, S. Chatterjee, S. Dehnen, *Adv. Opt. Mater.* **2019**, *7*, 1801793; d) N. W. Rosemann, J. P. Eußner, E. Dornsiepen, S. Chatterjee, S. Dehnen, *J. Am. Chem. Soc.* **2016**, *138*, 16224–16227; e) N. W. Rosemann, J. P. Eußner, A. Beyer, S. W. Koch, K. Volz, S. Dehnen, S. Chatterjee, *Science* **2016**, *352*, 1301–1304.
- [18] a) J.-P. Berndt, A. Engel, R. Hrdina, S. Dehnen, P. R. Schreiner, *Organometallics* **2019**, *38*, 329–335; b) N. Rinn, J.-P. Berndt, A. Kreher, R. Hrdina, M. Reinmuth, P. R. Schreiner, S. Dehnen, *Organometallics* **2016**, *35*, 3215–3220; c) A. Engel, S. Dehnen, *Eur. J. Inorg. Chem.* **2019**, 4313–4320; d) A. Engel, H. Dewald, A. Reuter, J. Klippstein, S. Dehnen, *Eur. J. Inorg. Chem.* **2020**, 2809–2815; e) A. Engel, E. Dornsiepen, S. Dehnen, *Inorg. Chem. Front.* **2019**, *6*, 1973–1976.
- [19] E. Geringer, E. Leusmann, F. Tambornino, M. Gerhard, M. Koch, S. Dehnen, *Chem. Commun.* **2020**, *56*, 4769–4772.
- [20] a) E. Leusmann, M. Wagner, N. W. Rosemann, S. Chatterjee, S. Dehnen, *Inorg. Chem.* **2014**, *53*, 4228–4233; b) E. Dornsiepen, S. Dehnen, *Eur. J. Inorg. Chem.* **2019**, 4306–4312; c) M. R. Halvagar, Z. Hassanzadeh Fard, S. Dehnen, *Chem. Eur. J.* **2011**, *17*, 4371–4374; d) A. Mishra, A. Betal, N. Pal, R. Kumar, P. Lama, S. Sahu, R. K. Metre, *ACS Appl. Electron. Mater.* **2020**, *2*, 220–229.
- [21] E. Leusmann, F. Schneck, S. Dehnen, *Organometallics* **2015**, *34*, 3264–3271.
- [22] E. Leusmann, N. W. Rosemann, B. Weinert, S. Chatterjee, S. Dehnen, *Eur. J. Inorg. Chem.* **2016**, 5300–5304.
- [23] a) B. E. K. Barth, E. Leusmann, K. Harms, S. Dehnen, *Chem. Commun.* **2013**, *49*, 6590–6592; b) E. Leusmann, E. Geringer, B. Weinert, S. Dehnen, *Dalton Trans.* **2016**, *45*, 15298–15302.
- [24] J. P. Eußner, B. E. K. Barth, E. Leusmann, Z. You, N. Rinn, S. Dehnen, *Chem. Eur. J.* **2013**, *19*, 13792–13802.
- [25] Z. You, S. Dehnen, *Inorg. Chem.* **2013**, *52*, 12332–12334.
- [26] Z. H. Fard, L. Xiong, C. Müller, M. Hołyńska, S. Dehnen, *Chem. Eur. J.* **2009**, *15*, 6595–6604.
- [27] B. M. Schmidt, M. Dräger, K. Jurkschat, *J. Organomet. Chem.* **1991**, *410*, 43–52.
- [28] a) B. E. K. Barth, B. A. Tkachenko, J. P. Eußner, P. R. Schreiner, S. Dehnen, *Organometallics* **2014**, *33*, 1678–1688; b) Z. H. Fard, M. R. Halvagar, S. Dehnen, *J. Am. Chem. Soc.* **2010**, *132*, 2848–2849.
- [29] K. Jurkschat, S. van Dreumel, G. Dyson, D. Dakternieks, T. J. Bastow, M. E. Smith, M. Dräger, *Polyhedron* **1992**, *11*, 2747–2755.
- [30] A. F. L. O. M Santos, J. A. S. A. Oliveira, M. J. S. Monte, *J. Chem. Thermodyn.* **2015**, *90*, 282–293.
- [31] X. Sheng, A. Peng, H. Fu, J. Yao, *Colloids Surf. A* **2007**, *308*, 136–140.
- [32] Z. Hassanzadeh Fard, C. Müller, T. Harmening, R. Pöttgen, S. Dehnen, *Angew. Chem. Int. Ed.* **2009**, *48*, 4441–4444; *Angew. Chem.* **2009**, *121*, 4507–4511.
- [33] Stoe and Cie GmbH, *X-Area*, **2016**.
- [34] G. M. Sheldrick, *Acta Crystallogr. Sect. A* **2015**, *71*, 3–8.
- [35] G. M. Sheldrick, *Acta Crystallogr. Sect. C* **2015**, *71*, 3–8.
- [36] O. V. Dolomanov, L. J. Bourhis, R. J. Gildea, J. A. K. Howard, H. Puschmann, *J. Appl. Crystallogr.* **2009**, *42*, 339–341.

Manuscript received: August 23, 2020

Revised manuscript received: September 16, 2020

Accepted manuscript online: September 16, 2020

Version of record online: December 17, 2020